ACS APPLIED MATERIALS & INTERFACES

Research Article

Cite This: ACS Appl. Mater. Interfaces 2018, 10, 2083−2092

www.acsami.org

In Situ Alloying of Thermally Conductive Polymer Composites by Combining Liquid and Solid Metal Microadditives

Matthew I. Ralphs, Nicholas Kemme, Prathamesh B. Vartak, Emil Joseph, Sujal Tipnis, Scott Turnage, Kiran N. Solanki, Robert Y. Wang,* and Konrad Rykaczewski*

School for Engineering of Matter, Transport, and Energy, Arizona State University, Tempe, Arizona 85287, United States

Supporting Information

ABSTRACT: Room-temperature liquid metals (LMs) are attractive candidates for thermal interface materials (TIMs) because of their moderately high thermal conductivity and liquid nature, which allow them to conform well to mating surfaces with little thermal resistance. However, gallium-based LMs may be of concern due to the gallium-driven degradation of many metal microelectronic components. We present a three-component composite with LM, copper (Cu) microparticles, and a polymer matrix, as a cheaper, noncorrosive solution. The solid copper particles alloy with the gallium in the LM, in situ and at room temperature, immobilizing the LM and eliminating any corrosion issues of nearby components. Investigation of the structure−property−process relationship of the three-component composites reveals that the method and degree of additive blending dramatically alter the resulting thermal transport properties. In particular, microdispersion of any combination of the LM and Cu additives results in a large number of interfaces and a thermal conductivity below 2 W m^{-1} K^{-1}. In contrast, a shorter blending procedure of premixed LM and Cu particle colloid into the polymer matrix yields a composite with polydispersed filler and effective intrinsic thermal conductivities of up to 17 W m^{-1} K^{-1} (effective thermal conductivity of up to 10 W m^{-1} K^{-1}). The LM−Cu colloid alloying into $CuGa_2$ provides a limited, but practical, time frame to cast the uncured composite into the desired shape, space, or void before the composite stiffens and cures with permanent characteristics.

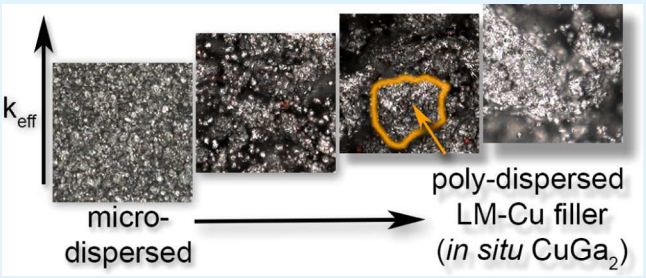

KEYWORDS: *liquid metal, thermal conductivity, in situ alloying, polymer composite, thermal interface material, particulate filler, copper, galinstan*

1. INTRODUCTION

Thermal management of integrated circuits (ICs) has become a limiting factor for transistor frequency, which has stalled around a few gigahertz over the past decade.[1,2] The large thermal loads stem from extremely densely packed, nanometer-sized features of modern ICs,[2−4] which provide minimal surface area for dissipation of the generated heat. This limitation has motivated the development of novel materials that can more efficiently conduct heat away from such hotspots.

Thermal interface materials (TIMs) play an integral role in dissipating heat away from ICs. Specifically, TIMs minimize the thermal contact resistance between electronic packaging components, such as processors and heat sinks, which stems from air gaps formed by surface mismatches of the two mating components. TIMs eliminate these air gaps by filling the geometrical imperfections with materials that have a high thermal conductivity (k). Some of the best performing commercial TIMs consist of thin metal foils with moderately low melting temperatures (T_{melt}) such as indium (T_{melt} = 157 °C, $k \approx 80$ W m^{-1} K^{-1}) or alloys such as SnBi (T_{melt} = 138 °C, $k \approx 20$ W m^{-1} K^{-1}).[5,6] However, these relatively low melting temperature materials have low mechanical compliance (as compared to that of, for example, polymer composites), which results in thermal fatigue in the IC because of the large mismatch in coefficients of thermal expansion between IC components.[7,8] This issue, along with the higher temperature required to melt and apply the indium and related films, makes room-temperature liquid metals (LMs) attractive alternatives. LMs have inherently good mechanical compliance because of their liquid state at normal IC operating temperatures.

Although a TIM made up of an array of mercury microdroplets has been described,[9] the limit of 100 ppm of mercury in any piece of electronic equipment (as dictated by the European Union's Restriction of Hazardous Substances Directive[10]), as well as general toxicity concerns, discourages the use of this metal. These limitations make gallium-based eutectic alloys such as GaIn (T_{melt} = 15.5 °C, $k \approx 32−39$ W m^{-1} K^{-1}) or GaInSn (T_{melt} = −19 °C, $k \approx 16−39$ W m^{-1} K^{-1}) much more practical for use in a TIM.[11−19] TIMs consisting of such LMs are commercially available, and several methods have been recently proposed to improve their thermal properties and wettability.[14,15]

Received: October 17, 2017
Accepted: December 13, 2017
Published: December 13, 2017

DOI: 10.1021/acsami.7b15814
ACS Appl. Mater. Interfaces 2018, 10, 2083−2092

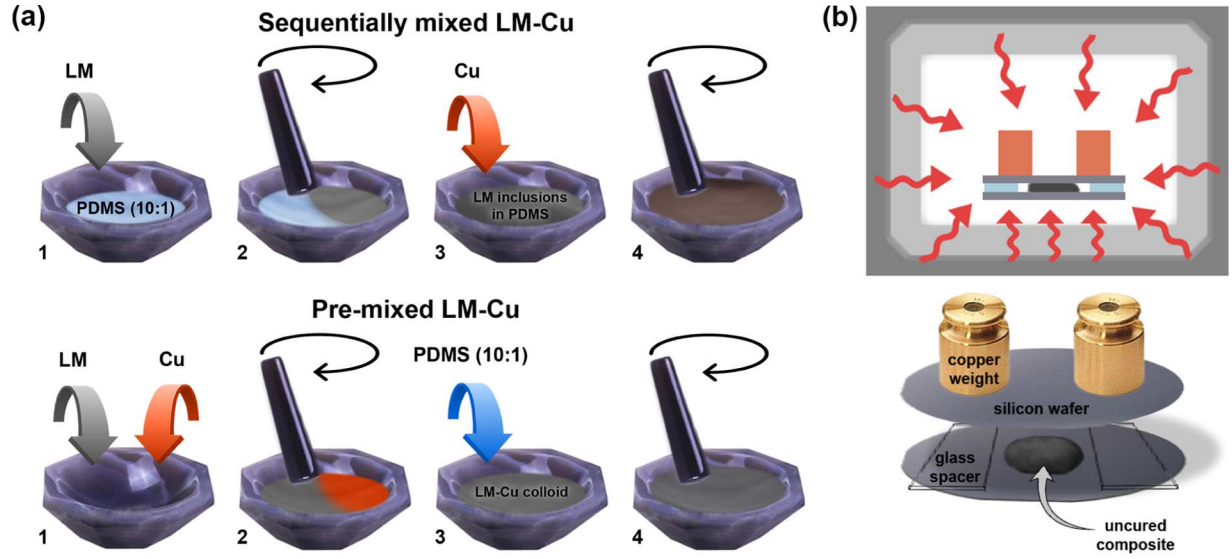

Figure 1. Schematic demonstrating the (a) difference between sequential mixing and premixing of liquid metal (LM) and copper microparticles (Cu) prior to blending into the PDMS matrix and (b) remaining fabrication procedure consisting of molding and curing.

One major concern with gallium-based LMs being used in TIMs for ICs is the rapid gallium-induced degradation of many metals used in IC packaging.[20−22] This concern is particularly severe with aluminum (one of the most common heat sink materials), which becomes extremely brittle when exposed to gallium.[21] To prevent corrosion, the mating materials can be modified through surface treatments (e.g., anodizing or introducing a tungsten barrier layer[23]), but, alternatively, gallium can be encapsulated and immobilized in a polymer matrix. This encapsulation process also resolves so-called pump-out issues, whereby voids (and correspondingly, hotspots) are created when the liquid metal is squeezed out from the gap during thermal cycling-induced device warping (see illustrative images of liquid metal side-leakage under minor compression in the Supporting Information, Figure S7).

To make polymers attractive as TIMs, thermally conductive particles are commonly added as fillers to increase the inherently low thermal conductivity of the matrix.[24−28] While the addition of many advanced materials such as carbon nanotubes, graphene, metal nanowires, boron nitride, and others has been recently investigated,[1,29−37] the majority of commercial TIMs rely on lower-cost ceramic or metal additives such as silver flakes, alumina, and graphite.[38,39] In nearly all cases, however, the effective intrinsic thermal conductivity of the composite, k, is limited by interface thermal resistances. These interface thermal resistances exist between the particles and the matrix and, when the percolation threshold is crossed, between the particle−particle contacts. Recent work has shown that k can be increased either by decreasing the particle−particle resistance (e.g., by microwave welding[31,40]) or by decreasing the number of interfaces through the matrix (e.g., by alignment of long particles[41−44]). Using LM as filler in a poly(dimethylsiloxane) (PDMS) matrix, Bartlett et al.[45] demonstrated that a high directional thermal conductivity of up to 10 W m^{-1} K^{-1} can be achieved by strain-induced spherical-to-cylindrical deformation of the microscale LM inclusions. Unfortunately, surface leakage of LM is a problem when composites with large LM inclusions[45−47] are cut or compressed (as with typical TIM applications). These types of mechanical forces drive the LM out of the polymer matrix (see Figure S5a in the Supporting Information) and hence Ga-induced corrosion of adjacent materials is still a concern.

In this work, we seek to simultaneously resolve the LM leakage issue and enhance the thermal properties of the composite by embedding both LM inclusions and copper (Cu) microparticles in a polymer matrix. In these three-component composites, the LM "glues" the copper particles together and eventually solidifies via in situ alloying of the LM and Cu into crystalline $CuGa_2$. In other words, the presented filler material system can be viewed as a solder that is molten at room temperature but then solidifies via chemical reaction (as opposed to freezing). We assert that this effect increases percolation and improves thermal pathways through the composite, thus increasing k, as well as immobilizing the LM to prevent gallium-induced degradation of nearby components. We investigate the structure−property−process relationship of these three-component composites and discuss the physical mechanisms underlying their performance.

2. EXPERIMENTAL SECTION

2.1. Composite Fabrication. We fabricated the three-component composites using the procedure outlined by Fassler et al.[46] and Bartlett et al.[45] In particular, we manually mixed together the GaInSn LM (Rotometals), Cu microparticles (10 μm APS, Alfa Aesar), and the poly(dimethylsiloxane) matrix (PDMS, Sylgard 184 with 10:1 base-to-curing agent ratio by weight) with mortar and pestle (see Figure 1a). We then poured the mixture into an open silicon mold and cured it in an oven (see Figure 1b). We controlled particle dispersion using the mixing time. Because our goal was to maximize the thermal conductivity of the composite, all samples were made at a filler volume fraction of ϕ = 0.5, which is also the highest fraction tested by Bartlett et al.[45] We note that Jeong et al.[48] made LM nanodroplet−PDMS composites with ϕ up to 0.66; however, these samples were, comparatively, very brittle. In our own attempts to go higher than ϕ = 0.5, the samples became difficult to fabricate and handle. Additionally, because copper is the most thermally conductive constituent of our three-phase composites, we used the highest practical fraction of the copper particles (i.e., 25% Cu, 25% LM, and 50% PDMS for the three-phase composites). We found that higher than 25% Cu was difficult to fully manually premix into the LM.

DOI: 10.1021/acsami.7b15814
ACS Appl. Mater. Interfaces 2018, 10, 2083−2092

The casting mold consists of top and bottom silicon wafers with glass slide spacers that determine the sample thickness (see Figure 1b). To maintain contact between the silicon wafers and the glass spacers, which will ensure a constant thickness throughout the sample, we placed two 200 g weights on top of the mold assembly for the duration of the cure. All samples in this work were about 2 mm thick prior to compression during the thermal transport measurement. All samples were cured in an oven (Fisher Scientific Isotemp 280A) at 100 °C for 2 h.

We used two approaches to combine the LM and Cu additives with the PDMS matrix. We either sequentially mixed the additives into PDMS (LM followed by Cu) or premixed the LM and Cu together prior to dispersing them in PDMS, as illustrated in Figure 1a. The sequential additive mixing method results in predominantly isolated microfillers with minimal LM−Cu interactions. Conversely, the additive premixing method ensures maximal interaction between the LM and Cu. This method produces initially heterogeneous LM−Cu particles that spontaneously alloy into $CuGa_2$ over time and in situ.

2.2. Composite Characterization. We imaged the morphology of the composites using high-magnification optical microscopy (Zeiss Axio Zoom.V16) with an objective lens of 2.3×/0.57 FWD and 10.6 mm focal length (Zeiss PlanNeoFluar Z) as well as scanning electron microscopy (SEM) (Amray 1910 with field emission gun). Because of the microscopic size of the particles and ease of their differentiation through color, optical imaging of the polymer composites proved to be much more insightful than SEM images. Consequently, we present optical images of the polymer composite samples. For characterization of solidified LM−Cu alloy cross sections, which were mirror-polished using standard procedures,[49] we utilized SEM imaging as well as energy-dispersive X-ray (EDS) mapping (performed with electron beam energy of 15 keV and spot setting of −15 using an EDAX Apollo detector with Genesis software). X-ray diffraction (XRD) was performed using a PANalytical X'Pert PRO MRD with a Cu Kα X-ray source operating at 40 kV and 40 mA.

We used two image processing methods to quantify the extent of filler dispersion in the samples. For the samples with microdispersed spheroidlike fillers, we calculated an equivalent diameter, D_{EQ}, to evaluate particle size such that

$$D_{EQ} = \sqrt{\frac{4A_p}{\pi}} \tag{1}$$

where A_p is the area of the particles as identified with ImageJ. For the samples with strongly polydispersed LM−Cu fillers, however, determination of an equivalent diameter was not representative because of the highly random nature of the filler shapes. Consequently, for these samples, we report the particle area distribution (PAD). Furthermore, because the PAD is highly non-Gaussian (a large number of particles with small areas and a few particles with very large areas), we present the PAD in cumulative terms. Specifically, the cumulative particle area distribution corresponds to the summation of the particle areas, sorted from the smallest to the largest, up to a given area value. The distribution is normalized by the total cumulative area. As a representative measure of the cumulative particle area, we used the 50 percentile (referred to as $PAD_{50\%}$). For each sample, we analyzed 8−10 images of the surface at various locations and separated filler from matrix through manual thresholding.

We measured the thermal resistance of the samples using a stepped-bar apparatus (SBA),[50,51] which is based on the ASTM D5470 standard[52] for measuring the thermal resistance of thin materials. Our custom SBA includes a linear encoder and a load cell that measure sample thickness and pressure, respectively, during thermal resistance measurements. Figure S1a in the Supporting Information illustrates the measurement principle of the ASTM D5470 method. Measuring thermal conductivity fundamentally requires applying a known heat flux to a sample of known geometry and then measuring the temperature drop across the sample. In this method, a steady-state temperature gradient across the sample is created using a heat source and a heat sink. The sample is placed between two metallic reference bars of known cross-sectional area and thermal conductivity. To minimize errors from misalignment, the top bar has a larger cross section than that of the bottom bar.[50] The temperature distribution in the reference bars (measured via thermocouples in precision-machined holes along the reference bar lengths) is then used to measure the heat flux, q, in the bars. Because the system is well insulated, the measured heat flow through the bars is equal to the measured heat flow through the sample. Extrapolating the temperature distributions of the reference bars to the bar−sample interfaces allows the temperature drop across the sample, ΔT, to be determined. The measured thermal resistance, R_{th}, across the sample is then obtained with

$$R_{th} = \frac{\Delta T}{q} \tag{2}$$

This thermal resistance represents the summation of the sample's intrinsic thermal resistance, R_s, as well as the thermal contact resistance, R_c, between the sample and the reference bars (note that R_c is the sum of two contact resistances, the contact resistance between the top reference bar and the top of the sample, and the contact resistance between the bottom reference bar and the bottom of the sample). The samples are under pressure during thermal resistance measurements to minimize R_c, which will bring k_{eff} closer to the true k of the composite. Various loads are used to gauge sample properties, but the target pressure for the results of this study is 1.5 MPa, which is near the high end of the pressure range applicable to electronic cooling.[32]

The measured thermal resistances, R_{th}, can be converted into intrinsic thermal conductivity values if the sample thickness, t_c, and the sample contact resistance, R_c, are known. We obtained the sample thickness during our measurements via the linear encoder that is integrated into our stepped-bar apparatus thermal transport measurement system. We also estimated R_c of our samples by measuring the thermal resistance of several samples with varying thicknesses and extrapolating to zero thickness. We estimate the values for R_c to be approximately 1.2×10^{-4} and 8×10^{-5} m^2 K W^{-1} at 1.5 MPa for well-dispersed samples and less-dispersed samples, respectively. The single-side contact resistance, $R_c/2$, (4×10^{-5} m^2 K W^{-1}) is comparable to that of Si−Al interfaces at the same pressure (2×10^{-5} m^2 K W^{-1}).[53] With R_{th} and t_c known, the effective thermal conductivity can be calculated by

$$k_{eff} = \frac{t_c}{R_{th}} = \frac{t_c}{R_c + R_s} \tag{3}$$

This effective thermal conductivity includes the combined effects of the intrinsic sample resistance and the sample contact resistance. Consequently, the effective thermal conductivity is smaller than the intrinsic sample thermal conductivity. However, strictly speaking, we cannot describe our samples with a single intrinsic thermal conductivity value because many of our samples are heterogeneous with large inclusions of several hundred microns in size. Consequently, we describe them with an effective intrinsic thermal conductivity, $\bar{k}$, of the composite, which can be calculated via the following equation

$$\bar{k} = \frac{t_c}{R_{th} - R_c} \tag{4}$$

Because of the Mullins effect of PDMS,[54] which results in a change or relaxation of the modulus between the first and second loadings, each sample is measured only once and only with increasing pressure. We estimate that the overall measurement uncertainty in k_{eff} ranges from 4 to 6% (68% confidence). Additional uncertainty arises as the thermal conductivities of the sample and reference bars become more similar, and this corresponds to the higher end of the previously mentioned uncertainty range. We validated our thermal conductivity measurements against literature results on PDMS−liquid metal composites[45,48] (see Figure S1b in the Support Information). Our measured PDMS thermal conductivity of 0.27 ± 0.01 W m^{-1} K^{-1} also

DOI: 10.1021/acsami.7b15814
ACS Appl. Mater. Interfaces 2018, 10, 2083−2092

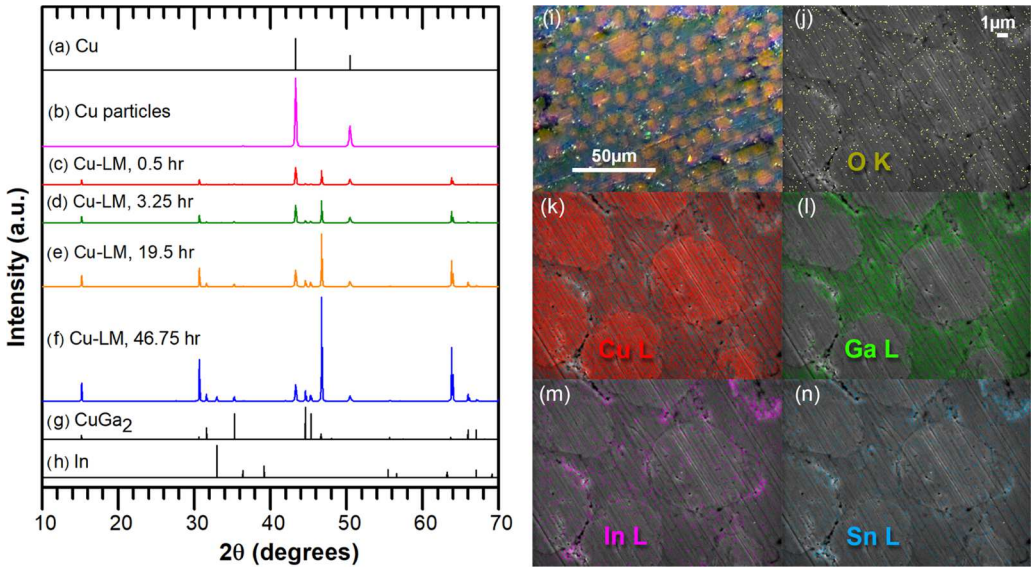

Figure 2. X-ray diffraction patterns of (a) Cu powder diffraction file 00-004-0836; (b) as-received Cu microparticles; LM−Cu mixtures (50:50 ratio) at (c) 0.5 h, (d) 3.25 h, (e) 19.5 h, and (f) 46.75 h after mixing; (g) $CuGa_2$ powder diffraction file 00-025-0275; and (h) In powder diffraction file 00-005-0642. An optical image (i) and a SEM image along with energy-dispersive X-ray spectroscopy (EDS) elemental maps (j−n) of a mirror-polished cross section of Cu particles mixed in LM at a 1:1 ratio 5 months after mixing.

matches well with the thermal conductivity stated by the manufacturer (Sylgard 184), 0.27 W m^{-1} K^{-1}.[55]

We also conducted a limited set of mechanical measurements. Specifically, we performed compressive relaxation tests on an INSTRON 5969 mechanical tester. Composites with large LM−Cu colloids have comparable properties to those of composites with 10 μm copper particles embedded in the PDMS matrix. Further details of the procedure and results of the mechanical tests can be found in the Supporting Information.

3. RESULTS AND DISCUSSION

3.1. LM−Cu Colloid and Alloy Characterization. Prior to discussing thermal properties of the polymer composites, we first discuss our material characterization of the LM−Cu colloid and $CuGa_2$ formation. Formation of the latter compound is thermodynamically favorable at room temperature, as illustrated in the Cu−Ga phase diagram,[56,57] and likely kinetically facilitated by the liquid state of the Ga in the LM. Indeed, X-ray diffraction (XRD) spectra presented in Figure 2 directly confirm $CuGa_2$ formation. In fact, Figure 2c shows that $CuGa_2$ diffraction peaks can be observed in as little as 30 min after mixing the Cu and LM together. Continual formation of $CuGa_2$ is also observed as the intensity ratio of the $CuGa_2$ peaks relative to the Cu peaks increases over time (Figure 2c−f). Extraction of Ga from the LM is also indirectly observed via the appearance of an In diffraction peak at 33.0° at 46.75 h (Figure 2f). This diffraction peak indicates the formation of crystalline In, which results due to LM solidification (i.e., extracting Ga from the LM changes the LM elemental composition and increases the melting temperature to above room temperature). Although this in situ alloying process is favorable from the perspective of immobilizing Ga and preventing damage to neighboring IC components, it also limits the time frame for shaping and molding the composites.[58] Markedly, mixing LM and Cu particles at a 1:1 ratio exhibits notable signs of hardening from $CuGa_2$ formation in under an hour, as observed in this study and by Hong and Suryanarayana.[59]

Because we are using a 50:50 ratio of Cu/LM, excess Cu remains after the formation of $CuGa_2$. This is evidenced by the presence of both Cu and $CuGa_2$ peaks in the XRD patterns. The In content in the LM is also revealed via the formation of the diffraction peak at 33.0° (Figure 2f). The presence of Sn in the LM is not directly detected by our XRD. This suggests that the Sn signal is too weak (the Sn content in our Cu/LM composite is just ∼3.5 atom %) or that Sn has dissolved/alloyed into one of the other metallic phases. Note that the colocation of Sn and In in the SEM EDS mapping (Figure 2m,n) suggests that Sn may have alloyed with the In phase; however, more precise characterization is needed to definitely confirm this hypothesis.

We used optical and SEM imaging as well as EDS mapping of the mirror-polished LM−Cu colloid cross section after full alloying occurred to evaluate the spatial distribution of $CuGa_2$ when Cu particles are mixed into LM at a 50:50 ratio. The results shown in Figure 2i−n clearly show that, at a 50:50 LM-to-Cu mixing ratio, the colloid alloys into a $CuGa_2$ matrix with the In, Sn, and O content surrounding Cu microparticles. Specifically, contrasting Cu and Ga distributions in Figure 2k,l indicates that Cu is mixing with the LM to form $CuGa_2$ in the space between pure Cu particles.

It is also important to acknowledge the effect of gallium oxide on the fabrication and performance of these composites. The LM−Cu colloids and all composites in this study were made in the presence of air, without any attempt to prevent LM oxidation. Gallium oxide forms readily on the surface of gallium-based LMs when exposed to even trace amount of oxygen and changes three main properties of the LM: viscosity, thermal conductivity, and wetting properties.[15,60,61] Specifically, when gallium oxide is present in the LM, the thermal conductivity of the resulting colloid (LM−solid oxide) is significantly decreased,[14,15,19] the viscosity significantly increased,[19,62] and the wetting properties are generally improved.[11,14,63,64] However, Li et al.[15] demonstrated that when Cu particles at ϕ_{Cu} = 0.07 are added to LM in the presence of oxygen (i.e., with oxide formation), the effective

DOI: 10.1021/acsami.7b15814
ACS Appl. Mater. Interfaces 2018, 10, 2083−2092

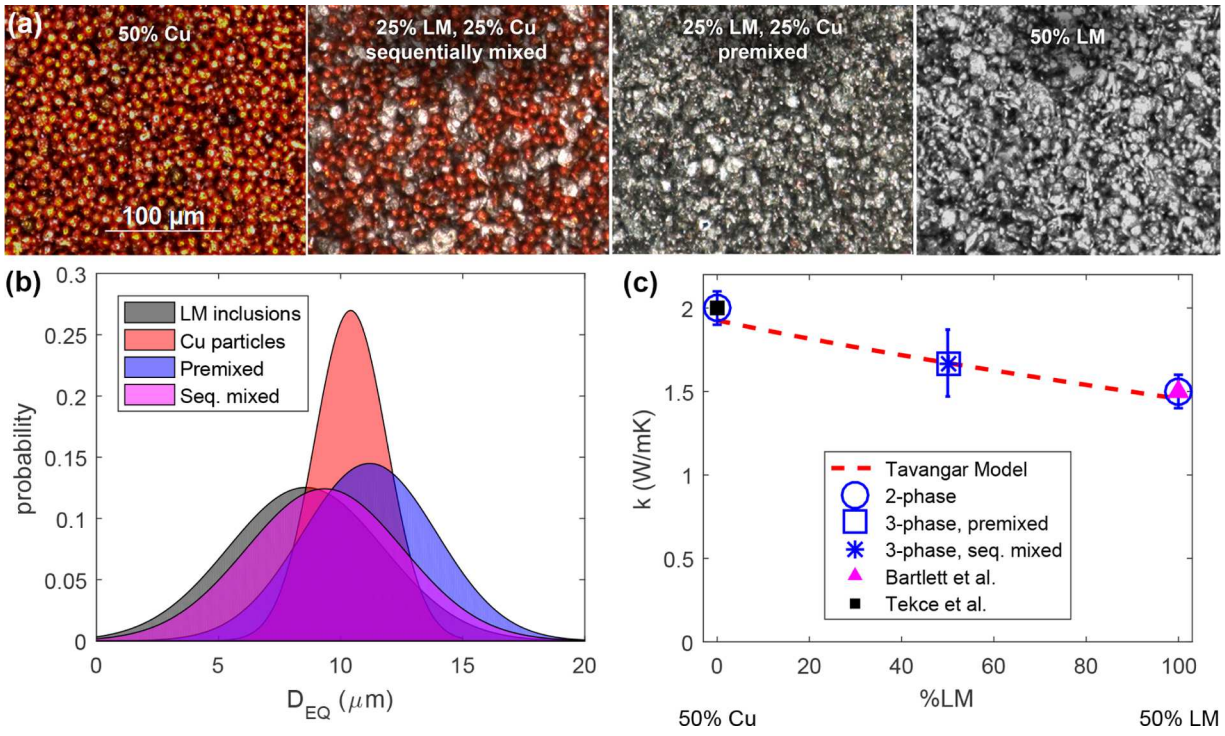

Figure 3. (a) Optical images of Cu-only PDMS, sequentially mixed LM−Cu−PDMS, premixed LM−Cu−PDMS, and LM-only PDMS composites at $\phi = 0.5$ with comparable inclusion size distributions, (b) plot of the particle size distributions where D_{EQ} is the equivalent diameter based on the particle and inclusion areas from image particle analysis, and (c) plots of the measured and theoretically predicted two-component and three-component composite thermal conductivities including literature data from Bartlett et al.[45] and Tekce et al.[68]

thermal conductivity of the colloid (LM with solid oxide and Cu which alloys into $CuGa_2$) is near that of pure LM. Taking into account that we use $\phi_{Cu} = 0.5$ in the LM colloid, the effect of oxide on the resulting thermal properties should be negligible. The Cu particles are likely well wetted by LM predominantly due to reactive wetting (via in situ alloying),[65] and not only by oxide formation. The oxide, however, forms on the surface of the colloid during blending into PDMS and likely facilitates the dispersion process.[61] It is also worth noting that, despite being only 1−2 nm thick, the oxide shell is strong enough to support free-standing LM structures[66] and even internal LM flow in pipes made out of oxide shells.[67] However, its presence is unlikely to have a major impact on mechanical properties of the three-phase composites once the alloying (i.e., solidification of the colloid) process occurs.

3.2. Thermal Properties of Composites with Micro-dispersed Fillers. We first evaluated the thermal properties of three-component composites with inclusion size distribution comparable to that of two-component Cu-only and LM-only composites. The images in Figure 3a show that the manual blending process can produce uniformly microdispersed Cu-only, LM-only, sequentially mixed LM−Cu, and premixed LM−Cu filler in the PDMS matrix. The particle size probability distribution plots in Figure 3b show that the manual blending process can produce LM microdroplets with $D_{EQ} = 8.6 \pm 3.2$ μm (68% confidence interval) and LM−Cu particles with $D_{EQ} = 11.2 \pm 2.8$ μm (for premixed) and 9.3 ± 3.2 μm (for sequentially mixed) close to that of the Cu particles ($D_{EQ} = 10.5 \pm 1.5$ μm). These probability distributions are fit from particle size distributions of the well-dispersed samples, assuming normal distributions (see Figure S2 in the Support Information). Because the particle distributions are similar in average size, the difference in the thermal conductivity of the composites should theoretically be predominantly determined by the thermal properties of the constituents and their volume fractions.

To predict the thermal conductivity of our composites, we start with the model as described by Tavangar[69] and add in a shape factor, L, to adjust for ellipsoidal LM inclusions when under load. The Tavangar model is a differential effective medium (DEM) scheme that accounts for interface thermal resistance between particles and the matrix and is fairly accurate at high-volume-fraction filler.[69,70] The Tavangar model is given as

$$1 - \phi = \frac{(k_m)^L(k_p k_c R_b + a k_c - a k_p)}{(k_c)^L(k_p k_m R_b + a k_m - a k_p)} \quad (5)$$

where L is the shape factor and is equal to 1/3 when the filler particles are spherical, k_p is the thermal conductivity of the particles or inclusions, k_m is the thermal conductivity of the matrix, k_c is the thermal conductivity of the composite, R_b is the interface thermal resistance, a is the radius of the particles (see the Supporting Information for the values of our specific inputs into the Tavangar model). Because the Tavangar model considers only composites with two components, we sequentially applied the Tavangar model for our composites with three components. More specifically, for our composites with PDMS, Cu, and LM, we first used the Tavangar model to calculate the thermal conductivity of a composite consisting of LM particles in a PDMS matrix, $k_{LM-PDMS}$. We then considered a composite consisting of Cu particles in a matrix and used $k_{LM-PDMS}$ as the matrix thermal conductivity, k_m, to yield the overall thermal conductivity of a Cu−LM−PDMS composite. Calculating k_c by adding LM into a Cu−PDMS matrix results in the same value as that obtained on adding Cu into a LM−

DOI: 10.1021/acsami.7b15814
ACS Appl. Mater. Interfaces 2018, 10, 2083−2092

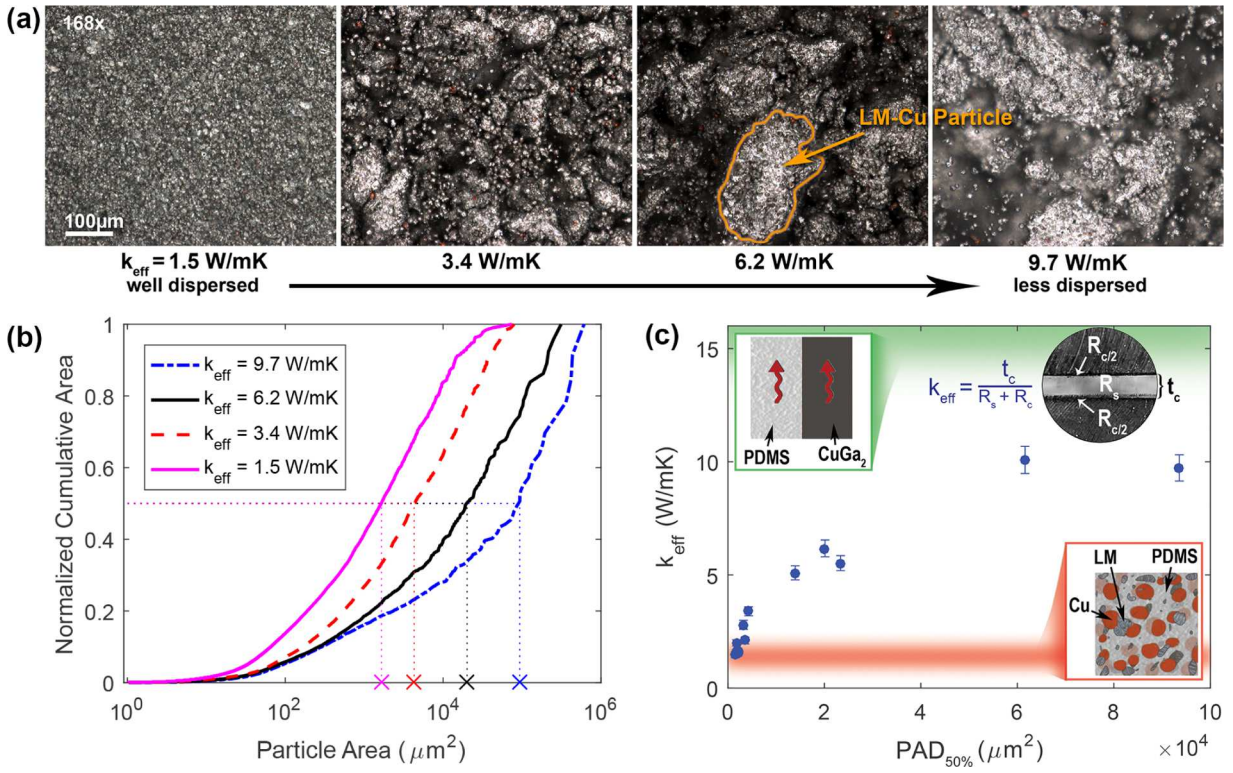

Figure 4. Premixed Cu–LM–PDMS composite structure–property–process results: (a) optical images of composites at 25% Cu, 25% LM, and 50% PDMS going from uniformly microdispersed on the left to highly polydispersed on the right, with their respective effective thermal conductivities; (b) normalized cumulative area distributions with indication of the 50th percentile ($PAD_{50\%}$) utilized to characterize each distribution; (c) effective thermal conductivity against the $PAD_{50\%}$ along with theoretical upper (green) and lower (red) bounds based on filler dispersion: from a block of $CuGa_2$ in parallel to a block of PDMS to microdispersed LM + Cu in PDMS.

PDMS matrix, but the latter sequence is used because it is the sequence whereby the actual samples are made.

Figure 3c shows measured and theoretically predicted values of k_c for the two-component and three-component composites as the ratio of LM to Cu is varied and ϕ is held constant at 0.5 (i.e., 50% PDMS and the other 50% is a ratio of LM and Cu). As predicted, the three-component composites have thermal conductivities in between 2.0 ± 0.1 W m^{-1} K^{-1} for the Cu-only PDMS composite and 1.5 ± 0.1 W m^{-1} K^{-1} for the LM-only PDMS composite. Specifically, the sequentially mixed and premixed LM–Cu–PDMS composites both have thermal conductivities of 1.65 ± 0.15 W m^{-1} K^{-1}. All of the measured composite thermal conductivities with well-dispersed fillers are about an order of magnitude higher than those of the matrix material (0.27 ± 0.01 W m^{-1} K^{-1}) and are comparable to previously described results.[45,68] These results demonstrate that increasing the thermal conductivity of the filler particles has diminishing returns. In particular, a 14-fold change in the thermal conductivity of the filler from 28 W m^{-1} K^{-1} for LM to 400 W m^{-1} K^{-1} for Cu results in only about a 1.3-fold increase in the thermal conductivity of the composite. Thus, substantial thermal conductivity enhancements can only be achieved by increasing the polymer thermal conductivity and/or improving the interfacial thermal transport (i.e., decreasing the number of interfaces and/or decreasing the thermal interface resistance).

3.3. Thermal Properties of Premixed Three-Phase Composites. Premixing the Cu particles into bulk LM provides a unique opportunity to enhance the composite thermal conductivity by decreasing the number of filler–PDMS boundaries via different levels of the LM–Cu colloid dispersion. Figure 4a shows that, by adjusting the manual blending time of the LM–Cu colloid into PDMS, we achieved dramatically different morphologies of the inclusions. In particular, decreasing the mixing time from 300 s (used for the microdispersed composites) to ~20–30 s results in a broad particle distribution with feature sizes ranging from a few microns to hundreds of microns. To quantify the filler dispersion in these samples, we used image processing to evaluate the particle cluster area distributions as described in Section 2.2. Figure 4b shows the normalized cumulative cluster area distributions corresponding to the example sample images in Figure 4a. In turn, Figure 4c presents the effective thermal conductivities of premixed LM–Cu–PDMS composites against their 50th percentile normalized cumulative cluster area distribution achieved through varied mixing times (see Section 2.2 for the reasoning behind the use of this distribution characteristic). These results demonstrate that retaining large fill structures within the matrix enhances thermal performance up to an effective thermal conductivity of 10 ± 0.6 W m^{-1} K^{-1} (or an effective intrinsic thermal conductivity of $\bar{k} \approx 17 \pm 3$ W m^{-1} K^{-1} if R_c is accounted for; see Figure S3 in the Supporting Information). One limitation to this work is that, although samples with such high thermal conductivity were repeatedly fabricated, it is difficult to fabricate them consistently because of variability associated with the short manual mixing time (we frequently observed a $k_{eff} \approx 4$–8 W m^{-1} K^{-1} for a short mixing time). These inconsistencies could be resolved by replacing the simple mortar and pestle mixing method outlined by Fassler et al.[46] and Bartlett et al.[45] with an alternate automated process.

DOI: 10.1021/acsami.7b15814
ACS Appl. Mater. Interfaces 2018, 10, 2083–2092

All of the thermal conductivity data in Figure 4c falls between the lower bound of uniformly microdispersed particles ($k_{eff} \approx 2$ W m^{-1} K^{-1}) and the upper bound of a two-part composite with 50% PDMS and 50% $CuGa_2$ ($k = 98$ W m^{-1} K^{-1})[71] blocks arranged in parallel ($k_{eff} \approx 16$ W m^{-1} K^{-1}, accounting for R_c of the same magnitude seen with our samples), as shown in the top left of Figure 4c.

We hypothesize that the thermal conductivity increase stems from two key factors: (i) the small thermal interface resistance of metal−metal interfaces with respect to that of the polymer−metal interfaces and (ii) the increased likelihood of percolation for large colloids relative to that for small colloids (i.e., the polydispersed colloids and well-dispersed colloids in this work, respectively). A review of the literature reveals that typical polymer−metal interfaces have thermal interface resistances of 10^{-6}−10^{-7} m^2 K W^{-1}, whereas typical metal−metal interfaces are several orders of magnitude lower (e.g., 2.5×10^{-10} m^2 K W^{-1} for an Al−Cu interface).[36,37,72] Consequently, we expect thermal transport through our $CuGa_2$−Cu interfaces to be orders of magnitude better than the transport through polymer−$CuGa_2$ or polymer−Cu interfaces.

It is also useful to analyze these numbers in the context of Kapitza lengths, $L_K = TBR \times k_{ref}$, where L_K, TBR, and k_{ref} are the Kapitza length, thermal boundary resistance, and reference thermal conductivity, respectively.[73] The Kapitza length relates the thermal boundary resistance to an equivalent slab of material with a thickness and thermal conductivity equivalent to L_K and k_{ref}. For example, a typical polymer−metal interface with TBR = 1×10^{-7} m^2 K W^{-1} poses a resistance equivalent to about 10 μm of $CuGa_2$ ($k_{CuGa_2} = 98$ W m^{-1} K^{-1}).[71] This value is significant because it is comparable to the 10 μm diameter of our well-dispersed particles (Figure 3b). Furthermore, considering that each particle has two heat transfer interfaces (i.e., going into and leaving the particle), thermal transport through the filler particles is bottlenecked by thermal transport through the polymer−particle interface. Relative to a polymer−metal interface, a typical metal−metal interface with TBR = 1×10^{-10} m^2 K W^{-1} poses a resistance equivalent to ∼0.01 μm of $CuGa_2$, which is negligibly small. This means that the internal Cu−$CuGa_2$ interfaces within our large LM−Cu colloids can be ignored and that these large colloids can be thought as large single particles with thermal conductivities on the order of 10^2 W m^{-1} K^{-1}. This high thermal conductivity should also allow these large particles to effectively short circuit around the low-thermal-conductivity PDMS ($k_{PDMS} = 0.27$ W m^{-1} K^{-1}).

We also hypothesize that the larger size of our polydispersed colloids with respect to that of our well-dispersed colloids (i.e., characteristic lengths of ∼100 and ∼ 10 μm, respectively) also plays a key role with respect to increased thermal conductivity. The classical percolation theory focuses on the probability of forming an infinite network in an infinite lattice. Naturally, such conditions are never perfectly achieved in the lab. Percolation studies on finite systems have shown that the percolation threshold decreases as a system becomes more finite.[74] This suggests that our larger colloids should more easily percolate than our smaller colloids. This is intuitive given our sample thickness, large colloid effective diameter, and small colloid effective diameter of ∼2 mm, ∼100 μm, and ∼ 10 μm, respectively. To a first approximation, percolation for our large colloids is a 20-body interaction and should be significantly more common than percolation for our small colloids, which is a 200-body interaction. Moreover, the thermal conductivity of the large colloid samples should also be improved because the thermal conductance for a percolating thread formed by ∼100 μm particles should be significantly larger than the thermal conductance for a percolating thread formed by ∼10 μm particles.

3.4. Ga Leakage and Corrosion Issues. Another benefit of the in situ $CuGa_2$ formation is that it immobilizes Ga, preventing any liquid leakage and associated corrosion of surrounding metals. This characteristic makes our composites safe to use with aluminum heat sinks and other metal components. Figure 5 shows a premixed composite sample pad after 40 h of being sandwiched between aluminum foil at 55 °C and 3 MPa (a) next to aluminum foil that was exposed to a drop of LM at room temperature for 24 h with no applied pressure (b, c). No macroscopic corrosion of the aluminum foil occurs with the premixed composite samples. Furthermore, to demonstrate that our samples can be applied with LM−Cu in the colloidal state, we cured a three-component sample in between two pieces of aluminum foil for 2 h at 100 °C (see Supporting Information). As in the previous case, we did not observe any evidence of corrosion of the aluminum foil. These results indicate that the affinity of Ga to Cu is sufficient to prevent Ga from leaching from the polymer and reacting with Al. Thus, the three-component composites should be safe to cure in place next to aluminum components.

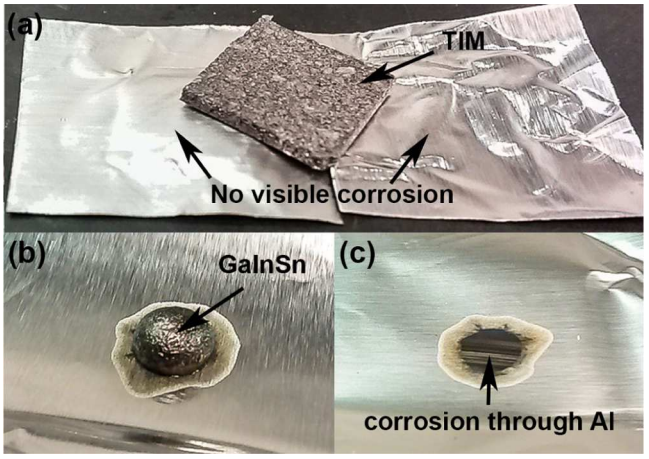

Figure 5. (a) 25% LM, 25% Cu, 50% PDMS sample made using the premixed method after being sandwiched between aluminum foil at 55 °C and 3 MPa for 40 h, (b) GaInSn on aluminum foil after 24 h at room temperature, and (c) the hole it corroded through the aluminum.

4. CONCLUSIONS

Our work demonstrates that gallium-based LMs have a great potential as filler in polymer TIMs once their leakage, and associated degradation of nearby components, is resolved. We showed that adding Cu particles as a third component to LM−polymer composites improves the chemical stability and effective thermal conductivity of the material over either two-component counterparts. The addition of Cu eliminates LM leakage from the composite via in situ $CuGa_2$ formation as well as by displacing the overall content of LM needed to achieve enhanced thermal conductivity. The formation of $CuGa_2$ is sufficiently slow to cast or mold this composite into any desired shape or void but fast enough to inhibit leaching of

DOI: 10.1021/acsami.7b15814
ACS Appl. Mater. Interfaces 2018, 10, 2083−2092

Ga to surrounding metals during the molding process. We note that, if found necessary, the rate of $CuGa_2$ formation could be altered through change of the sample processing temperature. Prevention of Ga leaching makes these composites safe to use with aluminum IC components.

Synergistically, the LM helps to glue or solder the Cu particles together forming LM−Cu colloids. The precoating of the Cu particles with LM facilitates the formation of large highly conductive filler structures that can more readily percolate and thermally short circuit through the polymer matrix. This leads to effective intrinsic thermal conductivity of up to 17 W m^{-1} K^{-1} ($k_{eff} \approx 10$ W m^{-1} K^{-1}) and represents a 10-fold improvement over the microdispersed composites with the same filler ratio and a 70-fold improvement over the polymer matrix itself.

■ ASSOCIATED CONTENT

Supporting Information

The Supporting Information is available free of charge on the ACS Publications website at DOI: 10.1021/acsami.7b15814.

Details of measurement and characterization techniques (PDF)

■ AUTHOR INFORMATION

Corresponding Authors

*E-mail: rywang@asu.edu (R.Y.W.).
*E-mail: konradr@asu.edu (K.R.).

ORCID

Konrad Rykaczewski: 0000-0002-5801-7177

Author Contributions

The manuscript was written through contributions of all authors. All authors have given approval to the final version of the manuscript.

Funding

M.I.R. acknowledges support through ASU's Fulton Schools of Engineering Dean's Fellowship. K.R. acknowledges startup funds from Fulton Schools of Engineering at ASU. P.B.V. and R.Y.W. acknowledge support from the National Science Foundation through award number DMR-1506829.

Notes

The authors declare no competing financial interest.

■ ACKNOWLEDGMENTS

We gratefully acknowledge the use of the facilities within the LeRoy Eyring Center for Solid State Science at Arizona State University.

■ REFERENCES

(1) Moore, A. L.; Shi, L. Emerging Challenges and Materials for Thermal Management of Electronics. *Mater. Today* **2014**, *17*, 163−174.

(2) *2015 International Technology Roadmap for Semiconductors (ITRS)*; Semiconductor Industry Association, 2015.

(3) Intel. Intel Xeon Processor E5-2695 v4. http://ark.intel.com/products/91316/Intel-Xeon-Processor-E5-2695-v4-45M-Cache-2_10-GHz.

(4) Ferain, I.; Colinge, C. A.; Colinge, J.-P. Multigate Transistors as the Future of Classical Metal−oxide−semiconductor Field-Effect Transistors. *Nature* **2011**, *479*, 310−316.

(5) Zhang, R.; Cai, J.; Wang, Q.; Li, J.; Hu, Y.; Du, H.; Li, L. Thermal Resistance Analysis of Sn-Bi Solder Paste Used as Thermal Interface Material for Power Electronics Applications. *J. Electron. Packag.* **2014**, *136*, No. 011012.

(6) Chung, D. D. Materials for Thermal Conduction. *Appl. Therm. Eng.* **2001**, *21*, 1593−1605.

(7) Blazej, D. Thermal Interface Materials. *Electron. Cool.* **2003**, *9*, 14−21.

(8) Bar-Cohen, A.; Matin, K.; Narumanchi, S. Nanothermal Interface Materials: Technology Review and Recent Results. *J. Electron. Packag.* **2015**, *137*, No. 040803.

(9) Hamdan, A.; McLanahan, A.; Richards, R.; Richards, C. Characterization of a Liquid−metal Microdroplet Thermal Interface Material. *Exp. Therm. Fluid Sci.* **2011**, *35*, 1250−1254.

(10) Directive 2011/65/EU of the European Parliament and the Council of 8 June 11 on the Restriction of the Use of Certain Hazardous Substances in Electrical and Electronic Equipment. *Off. J. Eur. Union* **2011**, *54* 88.

(11) Gao, Y.; Liu, J. Gallium-Based Thermal Interface Material with High Compliance and Wettability. *Appl. Phys. A* **2012**, *107*, 701−708.

(12) Roy, C. K.; Bhavnani, S.; Hamilton, M. C.; Johnson, R. W.; Knight, R. W.; Harris, D. K. Thermal Performance of Low Melting Temperature Alloys at the Interface between Dissimilar Materials. *Appl. Therm. Eng.* **2016**, *99*, 72−79.

(13) Roy, C. K.; Bhavnani, S.; Hamilton, M. C.; Johnson, R. W.; Knight, R. W.; Harris, D. K. Accelerated Aging and Thermal Cycling of Low Melting Temperature Alloys as Wet Thermal Interface Materials. *Microelectron. Reliab.* **2015**, *55*, 2698−2704.

(14) Gao, Y.; Wang, X.; Liu, J.; Fang, Q. Investigation on the Optimized Binary and Ternary Gallium Alloy as Thermal Interface Materials. *J. Electron. Packag.* **2016**, *139*, No. 011002.

(15) Li, G.; Ji, Y.; Wu, M.; Ma, H. In *Highly Conductive Thermal Paste of Liquid Metal Alloy Dispersed with Copper Particles*, Proceedings of the ASME 2016 Heat Transfer Summer Conference; American Society of Mechanical Engineers: Washington, DC, 2016.

(16) Plevachuk, Y.; Sklyarchuk, V.; Eckert, S.; Gerbeth, G.; Novakovic, R. Thermophysical Properties of the Liquid Ga−In−Sn Eutectic Alloy. *J. Chem. Eng. Data* **2014**, *59*, 757−763.

(17) Wilcox, M.; Ghoshal, U.; Grimm, D.; Ibrani, S.; Feicht, D.; Miner, A. High-performance liquid metal cooling loops. In *Semiconductor Thermal Measurement and Management Symposium*, 2005 IEEE Twenty First Annual IEEE; pp 19−19.

(18) Geratherm Medical AG. Safety Data Sheet for Galinstan fluid. http://www.rgmd.com/msds/msds.pdf (accessed Oct 6, 2017).

(19) Mei, S.; Gao, Y.; Deng, Z.; Liu, J. Thermally Conductive and Highly Electrically Resistive Grease Through Homogeneously Dispersing Liquid Metal Droplets Inside Methyl Silicone Oil. *J. Electron. Packag.* **2014**, *136*, No. 011009.

(20) Lyon, R. N. *Liquid Metals Handbook, The Committee on the Basic Properties of Liquid Metals*; Off. Nav. Res. Dep. Navy, 1952.

(21) Rajagopalan, M.; Bhatia, M. A.; Tschopp, M. A.; Srolovitz, D. J.; Solanki, K. N. Atomic-Scale Analysis of Liquid-Gallium Embrittlement of Aluminum Grain Boundaries. *Acta Mater.* **2014**, *73*, 312−325.

(22) Deng, Y. G.; Liu, J. Corrosion Development between Liquid Gallium and Four Typical Metal Substrates Used in Chip Cooling Device. *Appl. Phys. A: Mater. Sci. Process.* **2009**, *95*, 907−915.

(23) Ndieguene, A.; Albert, P.; Fortin, C.; Oberson, V.; Sylvestre, J. In *Eternal Packages: Liquid Metal Flip Chip Devices*, 2016 IEEE 66th Electronic Components and Technology Conference 2016; pp 580−587.

(24) Han, Z.; Fina, A. Thermal Conductivity of Carbon Nanotubes and Their Polymer Nanocomposites: A Review. *Prog. Polym. Sci.* **2011**, *36*, 914−944.

(25) Saba, N.; Tahir, P. M.; Jawaid, M. A Review on Potentiality of Nano Filler/natural Fiber Filled Polymer Hybrid Composites. *Polymers* **2014**, *6*, 2247−2273.

(26) Huang, X.; Jiang, P.; Tanaka, T. A Review of Dielectric Polymer Composites with High Thermal Conductivity. *IEEE Electr. Insul. Mag.* **2011**, *27*, 8−16.

DOI: 10.1021/acsami.7b15814
ACS Appl. Mater. Interfaces 2018, 10, 2083−2092

(27) Sarvar, F.; Whalley, D.; Conway, P. In *Thermal Interface Materials - A Review of the State of the Art*, 2006 1st Electronics Systemintegration Technology Conference, 2006; Vol. 2, pp 1292–1302.
(28) Hussain, F.; Hojjati, M.; Okamoto, M.; Gorga, R. E. Review Article: Polymer-Matrix Nanocomposites, Processing, Manufacturing, and Application: An Overview. *J. Compos. Mater.* **2006**, *40*, 1511–1575.
(29) Ralphs, M. I. *Investigating the Effect of Carbon Nanotube Functionalization in Polydimethylsiloxane Composite through Use of a Stepped Bar Apparatus*; Utah State University, 2016.
(30) Suh, D.; Moon, C. M.; Kim, D.; Baik, S. Ultrahigh Thermal Conductivity of Interface Materials by Silver-Functionalized Carbon Nanotube Phonon Conduits. *Adv. Mater.* **2016**, *28*, 7220–7227.
(31) Seshadri, I.; Esquenazi, G. L.; Borca-Tasciuc, T.; Keblinski, P.; Ramanath, G. Multifold Increases in Thermal Conductivity of Polymer Nanocomposites through Microwave Welding of Metal Nanowire Fillers. *Adv. Mater. Interfaces* **2015**, *2*, No. 1500186.
(32) Prasher, R. In *Thermal Interface Materials: Historical Perspective, Status, and Future Directions*, Proceedings of the IEEE; IEEE, 2006; Vol. *94*, pp 1571–1586.
(33) McNamara, A. J.; Joshi, Y.; Zhang, Z. M. Characterization of Nanostructured Thermal Interface Materials–a Review. *Int. J. Therm. Sci.* **2012**, *62*, 2–11.
(34) Wang, S.; Cheng, Y.; Wang, R.; Sun, J.; Gao, L. Highly Thermal Conductive Copper Nanowire Composites with Ultralow Loading: Toward Applications as Thermal Interface Materials. *ACS Appl. Mater. Interfaces* **2014**, *6*, 6481–6486.
(35) Zhu, H.; Li, Y.; Fang, Z.; Xu, J.; Cao, F.; Wan, J.; Preston, C.; Yang, B.; Hu, L. Highly Thermally Conductive Papers with Percolative Layered Boron Nitride Nanosheets. *ACS Nano* **2014**, *8*, 3606–3613.
(36) Prasher, R. S.; Chiu, C.-P. Thermal Interface Materials. *Materials for Advanced Packaging*; Springer, 2017; pp 511–535.
(37) Rai, A.; Moore, A. L. Enhanced Thermal Conduction and Influence of Interfacial Resistance within Flexible High Aspect Ratio Copper Nanowire/polymer Composites. *Compos. Sci. Technol.* **2017**, *144*, 70–78.
(38) Fu, Y. X.; He, Z. X.; Mo, D. C.; Lu, S. S. Thermal Conductivity Enhancement with Different Fillers for Epoxy Resin Adhesives. *Appl. Therm. Eng.* **2014**, *66*, 493–498.
(39) Yim, M. J.; Li, Y.; Moon, K.; Paik, K. W.; Wong, C. P. Review of Recent Advances in Electrically Conductive Adhesive Materials and Technologies in Electronic Packaging. *J. Adhes. Sci. Technol.* **2008**, *22*, 1593–1630.
(40) Seshadri, I.; Esquenazi, G. L.; Cardinal, T.; Borca-Tasciuc, T.; Ramanath, G. Microwave Synthesis of Branched Silver Nanowires and Their Use as Fillers for High Thermal Conductivity Polymer Composites. *Nanotechnology* **2016**, *27*, No. 175601.
(41) Balachander, N.; Seshadri, I.; Mehta, R. J.; Schadler, L. S.; Borca-Tasciuc, T.; Keblinski, P.; Ramanath, G. Nanowire-Filled Polymer Composites with Ultrahigh Thermal Conductivity. *Appl. Phys. Lett.* **2013**, *102*, No. 093117.
(42) Xie, X. L.; Mai, Y. W.; Zhou, X. P. Dispersion and Alignment of Carbon Nanotubes in Polymer Matrix: A Review. *Mater. Sci. Eng., R* **2005**, *49*, 89–112.
(43) Taphouse, J. H.; Bougher, T. L.; Singh, V.; Abadi, P. P. S. S.; Graham, S.; Cola, B. A. Carbon Nanotube Thermal Interfaces Enhanced with Sprayed on Nanoscale Polymer Coatings. *Nanotechnology* **2013**, *24*, No. 105401.
(44) Marconnet, A. M.; Yamamoto, N.; Panzer, M. A.; Wardle, B. L.; Goodson, K. E. Thermal Conduction in Aligned Carbon Nanotube-Polymer Nanocomposites with High Packing Density. *ACS Nano* **2011**, *5*, 4818–4825.
(45) Bartlett, M. D.; Kazem, N.; Powell-palm, M. J.; Huang, X.; Sun, W.; Malen, J. A.; Majidi, C. High Thermal Conductivity in Soft Elastomers with Elongated Liquid Metal Inclusions. *Proc. Natl. Acad. Sci. U.S.A.* **2017**, *114*, 2143–2148.
(46) Fassler, A.; Majidi, C. Liquid-Phase Metal Inclusions for a Conductive Polymer Composite. *Adv. Mater.* **2015**, *27*, 1928–1932.
(47) Bartlett, M. D.; Fassler, A.; Kazem, N.; Markvicka, E. J.; Mandal, P.; Majidi, C. Stretchable, High-K Dielectric Elastomers through Liquid-Metal Inclusions. *Adv. Mater.* **2016**, *28*, 3726–3731.
(48) Jeong, S. H.; Chen, S.; Huo, J.; Gamstedt, E. K.; Liu, J.; Zhang, S.-L.; Zhang, Z.-B.; Hjort, K.; Wu, Z. Mechanically Stretchable and Electrically Insulating Thermal Elastomer Composite by Liquid Alloy Droplet Embedment. *Sci. Rep.* **2015**, *5*, No. 18257.
(49) Doudrick, K.; Chinn, J.; Williams, J.; Chawla, N.; Rykaczewski, K. Rapid Method for Testing Efficacy of Nano-Engineered Coatings for Mitigating Tin Whisker Growth. *Microelectron. Reliab.* **2015**, *55*, 832.
(50) Thompson, D. R.; Rao, S. R.; Cola, B. a. A Stepped-Bar Apparatus for Thermal Resistance Measurements. *J. Electron. Packag.* **2013**, *135*, No. 041002.
(51) Ralphs, M. I.; Smith, B. L.; Roberts, N. A. Technique for Direct Measurement of Thermal Conductivity of Elastomers and a Detailed Uncertainty Analysis. *Meas. Sci. Technol.* **2016**, *27*, No. 115014.
(52) ASTM D5470. *Standard Test Method for Thermal Transmission Properties of Thermally Conductive Electrically Insulating Materials*; ASTM International, 2006.
(53) Ohsone, Y.; Dryden, J.; et al. Optical Measurement of Thermal Contact Conductance between Wafer-like Thin Solid Samples. *J. Heat Transfer* **1999**, *121*, 954–963.
(54) Diani, J.; Fayolle, B.; Gilormini, P. A Review on the Mullins Effect. *Eur. Polym. J.* **2009**, *45*, 601–612.
(55) Dow Corning. Electronics Sylgard 184 Silicone Elastomer. *Product Datasheet* 2013; pp 1–3. http://www.dowcorning.com/DataFiles/090276fe80190b08.pdf (accessed Oct 10, 2017).
(56) Predel, B. *Cu-Ga (Copper Gallium)*; Springer, 1994.
(57) Li, J. B.; Ji, L. N.; Liang, J. K.; Zhang, Y.; Luo, J.; Li, C. R.; Rao, G. H. A Thermodynamic Assessment of the Copper-Gallium System. *Calphad* **2008**, *32*, 447–453.
(58) Tang, J.; Zhao, X.; Li, J.; Guo, R.; Zhou, Y.; Liu, J. Gallium-Based Liquid Metal Amalgams: Transitional-State Metallic Mixtures (TransM2ixes) with Enhanced and Tunable Electrical, Thermal, and Mechanical Properties. *ACS Appl. Mater. Interfaces* **2017**, *9*, 35977–35987.
(59) Hong, S. J.; Suryanarayana, C. Mechanism of Low-Temperature Cu Ga 2 Phase Formation in Cu-Ga Alloys by Mechanical Alloying. *J. Appl. Phys.* **2004**, *96*, 6120–6126.
(60) Dickey, M. D.; Chiechi, R. C.; Larsen, R. J.; Weiss, E. A.; Weitz, D. A.; Whitesides, G. M. Eutectic Gallium-Indium (EGaIn): A Liquid Metal Alloy for the Formation of Stable Structures in Microchannels at Room Temperature. *Adv. Funct. Mater.* **2008**, *18*, 1097–1104.
(61) Doudrick, K.; Liu, S.; Mutunga, E. M.; Klein, K. L.; Damle, V.; Varanasi, K. K.; Rykaczewski, K. Different Shades of Oxide: From Nanoscale Wetting Mechanisms to Contact Printing of Gallium-Based Liquid Metals. *Langmuir* **2014**, *30*, 6867.
(62) Scharmann, F.; Cherkashinin, G.; Breternitz, V.; Knedlik, C.; Hartung, G.; Weber, T.; Schaefer, J. A. Viscosity Effect on GaInSn Studied by XPS. *Surf. Interface Anal.* **2004**, *36*, 981–985.
(63) Liu, T.; Sen, P.; Kim, C. J. Characterization of Nontoxic Liquid-Metal Alloy Galinstan for Applications in Microdevices. *J. Microelectromech. Syst.* **2012**, *21*, 443–450.
(64) Kazem, N.; Hellebrekers, T.; Majidi, C. Soft Multifunctional Composites and Emulsions with Liquid Metals. *Adv. Mater.* **2017**, *29*, No. 1605985.
(65) Kramer, R. K.; Boley, J. W.; Stone, H. A.; Weaver, J. C.; Wood, R. J. Effect of Microtextured Surface Topography on the Wetting Behavior of Eutectic Gallium-Indium Alloys. *Langmuir* **2014**, *30*, 533–539.
(66) Dickey, M. D. Emerging Applications of Liquid Metals Featuring Surface Oxides. *ACS Appl. Mater. Interfaces* **2014**, *6*, 18369–18379.
(67) Liu, S.; Sun, X.; Kemme, N.; Damle, V. G.; Schott, C.; Herrmann, M.; Rykaczewski, K. Can Liquid Metal Flow in

DOI: 10.1021/acsami.7b15814
ACS Appl. Mater. Interfaces 2018, 10, 2083–2092

Microchannels Made of Its Own Oxide Skin? *Microfluid. Nanofluid.* **2016**, *20*, 1−6.
(68) Tekce, H. S.; Kumlutas, D.; Tavman, I. H. Effect of Particle Shape on Thermal Conductivity of Copper Reinforced Polymer Composites. *J. Reinf. Plast. Compos.* **2007**, *26*, 113−121.
(69) Tavangar, R.; Molina, J. M.; Weber, L. Assessing Predictive Schemes for Thermal Conductivity against Diamond-Reinforced Silver Matrix Composites at Intermediate Phase Contrast. *Scr. Mater.* **2007**, *56*, 357−360.
(70) Pietrak, K.; Wisniewski, T. S. A Review of Models for Effective Thermal Conductivity of Composite Materials. *J. Power Technol.* **2015**, *95*, 14−24.
(71) Kulikova, T. V.; Bykov, V. A.; Shunyaev, K. Y.; Shubin, A. B. Thermal Properties of CuGa2 Phase in Inert Atmosphere. *Defect Diffus. Forum* **2012**, *326−328*, 227−232.
(72) Gundrum, B. C.; Cahill, D. G.; Averback, R. S. Thermal Conductance of Metal-Metal Interfaces. *Phys. Rev. B - Condens. Matter Mater. Phys.* **2005**, *72*, No. 245426.
(73) Cahill, D. G.; Ford, W. K.; Goodson, K. E.; Mahan, G. D.; Majumdar, A.; Maris, H. J.; Merlin, R.; Phillpot, S. R. Nanoscale Thermal Transport. *J. Appl. Phys.* **2003**, *93*, 793−818.
(74) Stauffer, D.; Aharony, A. *Introduction to Percolation Theory*, 2nd ed.; Taylor and Francis Inc., 1992.

DOI: 10.1021/acsami.7b15814
ACS Appl. Mater. Interfaces 2018, 10, 2083−2092